AIAA JOURNAL
Vol. 31, No. 6, June 1993

Systematic Comparison of Mathematically Simple Turbulence Models for Three-Dimensional Boundary Layers

Marco S. G. Bettelini* and Torstein K. Fanneløp†
Swiss Federal Institute of Technology, Zürich, 8092, Switzerland

The paper presents a systematic comparison of some widely used turbulence models with one another and with experiments. The mathematically simplest models applicable to three-dimensional steady, incompressible boundary layers are of primary interest. Besides the more widely used algebraic formulations, models using simplified transport equations for turbulence quantities, such as the Johnson-King model, are considered. These models are applied to a variety of well-established two-dimensional and three-dimensional test cases, for which accurate and reliable experimental data are available. To avoid differences associated with different numerical integration procedures, all models have been used with the same finite difference method especially developed for this purpose. This method solves the first-order boundary-layer equations written in terms of streamline coordinates. One broad conclusion of this study is that all models considered give reasonable predictions for the gross boundary-layer parameters, but important differences become apparent for certain local values. Specific recommendations for the choice of turbulence model in practical applications are included.

Introduction

A NEED for accurate but mathematically simple turbulence models will exist in the foreseeable future in spite of the rapid improvements in computer capacity and speed. Although recent progress in modeling and simulating turbulent flows has been remarkable, algebraic turbulence models still play a dominant role for boundary-layer computations. The main reason is that for most engineering problems algebraic closure models give reasonable predictions at very low cost. The apparent shortcomings of these models, e.g., in adverse pressure gradients, are often attributed to the "history" effects on the Reynolds shear stresses not accounted for in these simple equilibrium models. This is the reason for the strong interest in the model proposed by Johnson and King[1] for two-dimensional boundary layers. This model, although retaining most of the simplicity and cost-effectiveness of algebraic models, also allows explicitly for history effects in the development of the shear stresses.

The present study focuses on the mathematically simplest turbulence models for three-dimensional steady, incompressible boundary layers. The models considered are the more widely used algebraic formulations as well as models of the Johnson-King class, which use simplified transport equations for turbulence quantities. Because of their empirical nature, the turbulence models investigated should be verified by extensive comparisons with experimental data. To this end a large number of well-established test cases available in the literature are used. Our analysis is limited to the solution of the first-order boundary-layer equations. For the high Reynolds number flows considered and in the absence of separation, these equations suffice to describe the flowfield and can be solved with high accuracy.

An attempt has been made to give the study broad experimental support based on experimental results for a large number of flow configurations of interest for engineering applications. Great attention has been devoted to accurate definitions of the initial and boundary conditions required and to the numerical accuracy of the solution procedure. Overall our comparisons are believed to be more conclusive than previous studies based on a more restricted experimental basis or on computations carried out for "workshops" by different groups, using not only different turbulence models but also different numerical methods and small but significant differences in the initial and boundary conditions (see van den Berg et al.[2]).

In the present work streamline coordinates are used, with x_1 along the projection on the wall of the external velocity vector, x_2 in the wall plane perpendicular to x_1, and x_3 perpendicular to the wall. The mean velocity components and metric coefficients for the directions x_i are denoted by u_i and e_i, the curvatures of the x_i = const lines by K_i. As the boundary-layer thickness δ is assumed to be very small, e_3 can be chosen to be 1, so that x_3 denotes the physical wall distance. The extension of two-dimensional turbulence models to three-dimensional flows is often facilitated by the use of streamline coordinates.

II. Turbulence Models

The models considered herein are listed in Table 1. Although all of these models, but JK3, were formulated originally using an isotropic eddy-viscosity concept, they can easily be modified to account for anisotropy. Some models for the eddy-viscosity anisotropy are listed in Table 2. Only a brief presentation of the models considered is included herein. For more details and for a discussion of the physical assumptions involved in the models, the reader is referred to the original publications cited in Tables 1 and 2.

All of the models considered herein use the eddy-viscosity formulation

$$-\overline{u_i' u_3'} = \epsilon \frac{\partial u_i}{\partial x_3} \tag{1}$$

Table 1 Turbulence models studied

Name	Main references	Type
CF	Cebeci and Smith[3] Fanneløp and Humphreys[4]	Algebraic
BL	Baldwin and Lomax[5]	Algebraic
MI	Michel et al.[6]	Algebraic
JK	Johnson and King[1] Abid[7]	One-half equation
JK2	(new)	One-half equation
JK3	(new)	Two one-half equations

Received Dec. 11, 1991; revision received Sept. 13, 1992; accepted for publication Sept. 15, 1992.

*Research Engineer, Department of Fluid Dynamics.
†Professor, Department of Fluid Dynamics. Member AIAA.

Table 2 Models for the eddy-viscosity anisotropy [the additional model parameters (AMP) introduced are listed in the last column]

Model	ϵ_{11}/ϵ	ϵ_{12}/ϵ	ϵ_{21}/ϵ	ϵ_{22}/ϵ	AMP
Isotropic	1	0	0	1	—
Fanneløp-Humphreys[4]	1	0	0	E	E
Ryhming-Fanneløp[4]	$\left\|\frac{\partial u_1}{\partial x_3}\left(\frac{\partial u_1}{\partial x_3}\right)_\beta^{-1}\right\|$	0	0	$\left\|\frac{\partial u_2}{\partial x_3}\left(\frac{\partial u_2}{\partial x_3}\right)_\beta^{-1}\right\|$	—
Rotta[9,10]	$\frac{u_1^2+Au_2^2}{u_1^2+u_2^2}$	$\frac{(1-A)u_1u_2}{u_1^2+u_2^2}$	$\frac{(1-A)u_1u_2}{u_1^2+u_2^2}$	$\frac{u_2^2+Au_1^2}{u_1^2+u_2^2}$	A
Moreau-Rotta[11]	1	$-B$	B	1	B

where $i = 1, 2$ if isotropy of the eddy viscosity is assumed. This formulation can be extended to

$$-\overline{u_i' u_3'} = \epsilon_{i1}\frac{\partial u_1}{\partial x_3} + \epsilon_{i2}\frac{\partial u_2}{\partial x_3} \tag{2}$$

to account for the experimentally observed anisotropy of the eddy viscosity in three-dimensional boundary layers. Some of the expressions for the eddy-viscosity anisotropy used by the algebraic models are summarized in Table 2. All of the models, except Ref. 8, involve additional anisotropy parameters, the values of which are not specified by the model. The new parameters are listed in the last column of Table 2. Since they can vary over a wide range,[12] their specification is usually a major problem. In most cases the values will be empirical, to be extracted from available experimental data. The use of these models will be discussed in Sec. V.

The following algebraic models are studied:

Cebeci-Smith[3] and Fanneløp-Humphreys[4] (CF):

$$\epsilon = l^2\sqrt{\left(\frac{\partial u_1}{\partial x_3}\right)^2 + \left(\frac{\partial u_2}{\partial x_3}\right)^2} \qquad \text{for } x_3 < x_3^* \tag{3a}$$

$$\epsilon = 0.0168\, U_e\, \delta_3^* D\, \gamma \qquad \text{for } x_3 \geq x_3^* \tag{3b}$$

with

$$p = 0.41\, x_3\, D \tag{4a}$$

$$D = 1 - \exp\left(-\frac{u_\tau x_3}{26\nu}\right) \tag{4b}$$

$$\delta_{3D}^* = \int_0^\infty \left(1 - \frac{\sqrt{u_1^2+u_2^2}}{U_e}\right) dx_3 \tag{4c}$$

$$\gamma = \left[1 + 5.5\left(\frac{x_3}{\delta}\right)^6\right]^{-1} \tag{4d}$$

where x_3^* denotes the smallest wall distance x_3 for which the expressions (3a) and (3b) assume the same value. The variables U_e, δ, u_τ and ν denote the external velocity, the boundary-layer thickness, the friction velocity, and the kinematic viscosity respectively. For streamline coordinates and small cross-flows ($u_2 \ll u_1$), the parameter δ_{3D}^* will be approximately equal to the displacement thickness, also in three-dimensional flows (Lighthill[13] and Fanneløp[14]).

Baldwin-Lomax[5] (BL):

$$\epsilon = l^2\sqrt{\left(\frac{\partial u_1}{\partial x_3}\right)^2 + \left(\frac{\partial u_2}{\partial x_3}\right)^2} \qquad \text{for } x_3 < x_3^* \tag{5a}$$

$$\epsilon = 0.0168\, C_{CP}\, x_{3\,\max} F_{\max}\gamma' \qquad \text{for } x_3 \geq x_3^* \tag{5b}$$

with

$$C_{CP} = 1.6 \tag{6a}$$

$$\gamma' = \left[1 + 5.5\left(\frac{0.3x_3}{x_{3\,\max}}\right)^6\right]^{-1} \tag{6b}$$

where $F_{\max}$ and $x_{3\,\max}$ denote the maximum of the function

$$F = x_3\, D\sqrt{\left(\frac{\partial u_1}{\partial x_3}\right)^2 + \left(\frac{\partial u_2}{\partial x_3}\right)^2} \tag{6c}$$

and its location, respectively. The remaining symbols are as in the CF-model.

Michel et al.[6] (MI):

$$\epsilon = l^2\sqrt{\left(\frac{\partial u_1}{\partial x_3}\right)^2 + \left(\frac{\partial u_2}{\partial x_3}\right)^2} \tag{7}$$

with

$$\rho = 1.0.085\delta \tanh\left(\frac{0.41\, x_3}{0.085\,\delta}\right)D \tag{8}$$

The remaining symbols are as in the CF-model.

The models of the Johnson-King class use one or more highly simplified transport equations for the turbulent quantities in which the dependence on the wall distance has been dropped. As the influence of the evolution of turbulence on the Reynolds stresses is taken into account, albeit rather approximately, these models are expected to be more generally applicable than the algebraic formulations. The improved models can be easily introduced in most existing computer programs designed for algebraic models, and they do not involve significant increases in storage requirement or computing time. Three models are considered in this class.

Johnson-King[1] (JK):

This model is described in detail in Johnson and King.[1] The eddy-viscosity distribution is given by

$$\epsilon = \epsilon_o[1 - \exp(-\epsilon_i/\epsilon_0)] \tag{9}$$

with

$$\epsilon_i = 0.4D^2 x_3\sqrt{\tau_M} \tag{10a}$$

$$\epsilon_o = 0.0168 U_e \delta^* \gamma\sigma(x_1, x_2) \tag{10b}$$

where τ_M denotes the maximum resulting Reynolds shear stress parameter at the location x_1, x_2 considered. The subscript M denotes values at the wall distance $x_{3,M}$ at which this maximum occurs; σ depends on τ_M, which is computed using

$$u_{1,M}\frac{\partial \tau_M}{\partial x_1} + u_{2,M}\frac{\partial \tau_M}{\partial x_2} = \frac{a_1}{L}\tau_M[\sqrt{\tau_{M,\text{eq}}} - \sqrt{\tau_M}] - a_1 D_M \tag{11}$$

where $\tau_{M,eq}$ denotes the maximum resulting Reynolds shear stress parameter in the equilibrium case, which is computed assuming $\sigma = 1$ in Eq. (10b), and D_M is a modeled diffusion term. The value 0.25 is used for a_1, and L is given by

$$L = \begin{cases} 0.4x_{3,M} & \text{if } x_{3,M} < 0.225\delta \\ 0.09\delta & \text{if } x_{3,M} \geq 0.225\delta \end{cases}$$

The remaining symbols are as in the CF-model.

This three-dimensional form of the Johnson-King model was first used by Abid.[7] Full details on the original Johnson-King formulation are given in Johnson and King.[1]

JK2:

For unseparated boundary layers, the eddy-viscosity distribution given by Eq. (9) results often in too low Reynolds shear stresses in the near-wall region, e.g., in two-dimensional boundary layers in weak pressure gradients (Bettelini[15]). A simple modification is proposed that introduces a new empirical parameter n:

$$\epsilon = \epsilon_o[1 - \exp - (\epsilon_i/\epsilon_0)^n]^{1/n} \tag{12}$$

The functions ϵ_i and ϵ_o are unchanged and are given in Eq. (10). The value $n = 2$ is found to give better agreement with available experimental data for the flows considered herein. A practical advantage of this formulation is that the original JK eddy-viscosity distribution is easily recovered by setting $n = 1$ during a computation. This could be useful in calculations leading to separation, as $n \approx 1$ gives better agreement near separation.

JK3:

Detailed measurements of the Reynolds stresses and the mean flow profiles in three-dimensional boundary layers show that the proportionality between the stress and the mean rate of strain, i.e., the eddy viscosity, depends not only on position but also on direction. Specifically, the eddy viscosity in the crossflow direction is found to be much reduced, often to less than 50% of the value in the direction of the inviscid streamline. As a consequence, the vectors for the mean rate of strain and the local shear stress have different directions. The difference (mostly a few degrees) will depend on position and the upstream flow history.

In what follows we have chosen to model the flow-history effects on the shear-stress ratio τ_2/τ_1, i.e., crossflow-to-streamline Reynolds stresses. To this end the anisotropic model of Rotta[9,10] is reformulated. The Reynolds stress parameters are expressed as

$$-\overline{u_1' u_3'} = \epsilon\left[\frac{u_1^2 + Au_2^2}{u_1^2 + u_2^2}\frac{\partial u_1}{\partial x_3} + \frac{(1-A)u_1u_2}{u_1^2 + u_2^2}\frac{\partial u_2}{\partial x_3}\right] \tag{13a}$$

$$-\overline{u_2' u_3'} = \epsilon\left[\frac{(1-A)u_1u_2}{u_1^2 + u_2^2}\frac{\partial u_1}{\partial x_3} + \frac{Au_1^2 + u_2^2}{u_1^2 + u_2^2}\frac{\partial u_2}{\partial x_3}\right] \tag{13b}$$

A major problem is related to the specification of the anisotropy parameter A, usually assumed to be constant. Unfortunately, experimental data[12] show not only large variations of A for different experimental configurations but also nonnegligible spatial variations for a given experiment. In the present formulation a new semi-empirical equation for the computation of this parameter is proposed. The Reynolds shear stress and direction along the surface $x_{3,M}$ are computed by

$$\frac{u_{1,M}}{e_1}\frac{\partial \tau_M}{\partial x_1} + \frac{u_{2,M}}{e_2}\frac{\partial \tau_M}{\partial x_2} = a_1\left[\tau_1\left(c_{11}\frac{\partial u_1}{\partial x_3} + c_{12}\frac{\partial u_2}{\partial x_3}\right) + \tau_2\left(c_{21}\frac{\partial u_1}{\partial x_3} + c_{22}\frac{\partial u_2}{\partial x_3}\right)\right]_M - a_1\frac{\tau_M^{3/2}}{L} + \text{Diff.}(\tau_M) \tag{14}$$

$$\frac{u_{1,M}}{e_1}\frac{\partial(\tau_2/\tau_1)_M}{\partial x_1} + \frac{u_{2,M}}{e_2}\frac{\partial(\tau_2/\tau_1)_M}{\partial x_2} = a_1\left(\frac{\tau}{\tau_1}\right)_M\left[\left(c_{21}\frac{\partial u_1}{\partial x_3} + c_{22}\frac{\partial u_2}{\partial x_3}\right) - \frac{\tau_2}{\tau_1}\left(c_{11}\frac{\partial u_1}{\partial x_3} + c_{12}\frac{\partial u_2}{\partial x_3}\right)\right]_M + (K_2\,u_{1,M} - K_1\,u_{2,M})\left[1 + \left(\frac{\tau_2}{\tau_1}\right)_M^2\right] + \text{Diff.}\left(\frac{\tau_2}{\tau_1}\right)_M \tag{15}$$

with

$$\tau_i = -\overline{u_i' u_3'}$$

$$\tau = \sqrt{\tau_1^2 + \tau_2^2}$$

and

$$\begin{cases} c_{11} = \dfrac{u_1^2 + T\,u_2^2}{u_1^2 + u_2^2} \\ c_{12} = c_{21} = \dfrac{(1-T)u_1\,u_2}{u_1^2 + u_2^2} \\ c_{22} = \dfrac{T\,u_1^2 + u_2^2}{u_1^2 + u_2^2} \end{cases} \tag{16}$$

where T is a measure of the anisotropy of the "rapid" part of the pressure-strain correlation in the model proposed by Rotta.[9,10] As a first approximation, the diffusion terms Diff. (...) in Eqs. (14) and (15) are neglected. The anisotropy parameter A is assumed to be independent of the wall distance x_3 and is computed from the Reynolds shear stresses at the location $x_{3,M}$. From Eqs. (13a) and (13b) the ratio $(\tau_2/\tau_1)_M$ is formed, and A is expressed in terms of $(\tau_2/\tau_1)_M$, found from Eq. (15):

$$A = \frac{u_{1,M}\,u_{2,M} + (u_{2,M})^2 G - (\tau_2/\tau_1)_M[(u_{1,M}{}^2 + u_{1,M}\,u_{2,M}\,G]}{u_{1,M}\,u_{2,M} - (u_{1,M})^2 G + (\tau_2/\tau_1)_M[(u_{2,M})^2 - u_{1,M}\,u_{2,M}\,G]} \tag{17}$$

with

$$G = \left[\frac{\partial u_2}{\partial x_3}\left(\frac{\partial u_1}{\partial x_3}\right)^{-1}\right]_M$$

The computation proceeds along the same lines as for the original Johnson-King formulation, but the additional equation, Eq. (15), has to be solved in order to compute the anisotropy parameter A. The initial conditions for Eqs. (14) and (15) will be known either from available experimental data or by assuming equilibrium turbulent flow at the initial stations. In the latter case, the computation is started using $\sigma = 1$ in Eq. (10b) and $A = 1$ in Eq. (13). Numerical experiments have shown that the influence of the initial conditions on the results is not strong.

The derivation of Eqs. (14) and (15) is discussed in Bettelini.[15] For $T = 1$, Eq. (15) can be written in the form

$$u_{1,M}\frac{\partial(\tau_2/\tau_1)_M}{\partial x_1} + u_{2,M}\frac{\partial(\tau_2/\tau_1)_M}{\partial x_2} = a_1\sqrt{\left(\frac{\partial u_1}{\partial x_3}\right)^2 + \left(\frac{\partial u_2}{\partial x_3}\right)^2} \times\left[\left(\frac{\tau_2}{\tau_1}\right)_{M,eq} - \left(\frac{\tau_2}{\tau_1}\right)_M\right] + (K_2\,u_{1,M} - K_1\,u_{2,M}) \times\left[1 + \left(\frac{\tau_2}{\tau_1}\right)_M^2\right] + \text{Diff.}\left(\frac{\tau_2}{\tau_1}\right)_M \tag{18}$$

with

$$\left(\frac{\tau_2}{\tau_1}\right)_{M,eq} = \left[\frac{\partial u_2}{\partial x_3}\left(\frac{\partial u_1}{\partial x_3}\right)^{-1}\right]_M$$

In the two-dimensional limit, this model reduces to the well-tested JK formulation. Eddy-viscosity anisotropy has a pronounced effect on the crossflow velocity profile and wall shear, but the effect on the magnitude of the maximum Reynolds shear stress is rather weak. As a result, Eq. (14) can be replaced by Eq. (11), the simplest three-dimensional form of the original Johnson-King equation, without much loss in accuracy. This approximation has been used to obtain the results presented in Sec. V.

III. Test Cases

The test cases selected are listed in Table 3. They include some representative two-dimensional results and a wide selection of available three-dimensional experiments. Most of the two-dimensional test cases considered in this study involve adverse pressure gradients. This is because many turbulence models are known to perform poorly under such conditions, which are often of crucial interest in engineering applications. Most of the three-dimensional test cases chosen represent pressure-driven flows because of their great practical importance in both internal and external aerodynamics. In addition, two shear-driven flows, of interest in the design of turbomachinery, are also included. The computation of the initial and boundary conditions is presented in Bettelini.[15]

Only a few representative results of the many two- and three-dimensional cases studied are presented in this paper. The first test case shown is SAJO73. This is a nominally two-dimensional boundary-layer flow with an increasingly adverse pressure gradient. The external velocity distribution is presented in Fig. 1. The Reynolds number at $x/L = 1$ is 1.7×10^6/m. This experiment is described in detail in Samuel and Joubert.[19]

The case BEEL72 is presented as typical for the three-dimensional test cases shown. In this experiment the boundary layer in a flow analogous to that of an infinite swept wing is studied in great detail. The external flow is presented in Fig. 2. The coordinate x denotes here the distance from the leading edge of the experimental model, measured in the direction of the undisturbed flow upstream. The Reynolds number at the entry of the test section is 2.42×10^6/m. The streamwise pressure gradient is positive over the full region investigated and leads eventually to a three-dimensional separation at about $x/L = 1.3$. As the streamwise integration of the first-order boundary-layer equations in the "direct mode" leads to an ill-posed problem as separation is approached,[2] we present results only up to about $x/L = 1.1$. Full details on BEEL72 are given in van den Berg et al.[21] The comparison with the POBR82 data, an independent realization of the same flow configuration, leads to essentially identical conclusions.

Table 3 Test cases considered

Class	Identification	Main references
Two dimensional	WITI44	Wieghardt and Tillmann[16]
	SCKL50	Schubauer and Klebanoff[17]
	CLAU54	Clauser[18]
	SAJO73	Samuel and Joubert[19]
	GATH92	Gasser[20] (Thomann)
Infinite swept wing	BEEL72	van den Berg et al.[21]
	POBR82	Bradshaw and Pontikos[22]
Wing-body junction	DEFE77	Dechow and Felsch[23] Felsch et al.[24]
	KRFA79	Krogstad[25] (Fanneløp)
Three-dimensional pressure field	MUKR79	Müller[26] (Krause)
	TRRY90	Truong[27] (Ryhming)
Shear driven	BIME70	Bissonnette and Mellor[28]
	LOHM73	Lohmann[29]

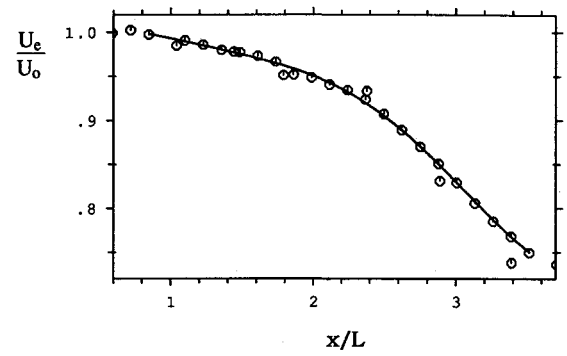

Fig. 1 SAJO73: dimensionless external velocity U_e.

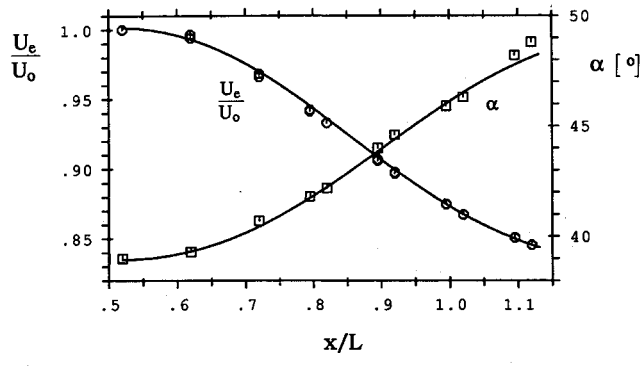

Fig. 2 BEEL72: dimensionless external velocity U_e and flow angle α (measured with respect to the undisturbed flow direction upstream of the wing, in degrees).

IV. Numerical Method

The first-order boundary-layer equations are solved in the direct mode by means of a modern version of an implicit finite difference technique used by Fanneløp[30] and Fanneløp and Humphreys[4] and described in detail in Bettelini.[15] This method has first-order accuracy in the streamwise direction and second-order accuracy in the crossflow and wall-normal directions. The scheme satisfies the consistency requirement and is unconditionally stable, according to a von Neumann analysis. Numerical convergence was verified for all of the computations by varying the step sizes in all directions by a factor of at least 1.5 to 2. The grid points were equally spaced in the streamwise direction and followed a geometric progression in the wall-normal direction, with a maximum stretching of about 1000 between the wall and the edge of the computational domain. The computation of SAJO73 was carried out using 200 grid points in the wall-normal direction and about 270 steps in the streamwise direction. The corresponding values for BEEL72 were 150 and 230. The computing times for all models presented were on the order of a few seconds on a CDC Cyber 180-855.

V. Results

Results for all of the test cases listed in Table 3 are presented in Bettelini.[15] In this paper only a few representative results for SAJO73 and BEEL72 are included, but the conclusions to be presented depend on all cases considered and on comparisons with all of the available experimental data. In all diagrams presented, the experimental values are indicated by points, and the computations are represented by lines.

An acceptable turbulence model for three-dimensional boundary layers must perform satisfactorily also in the two-dimensional limit. For this reason some two-dimensional results are first presented and discussed. Figures 3 and 4 show the mean velocity and Reynolds stress profiles for SAJO73. In this case the mean velocity profiles are not very sensitive to the

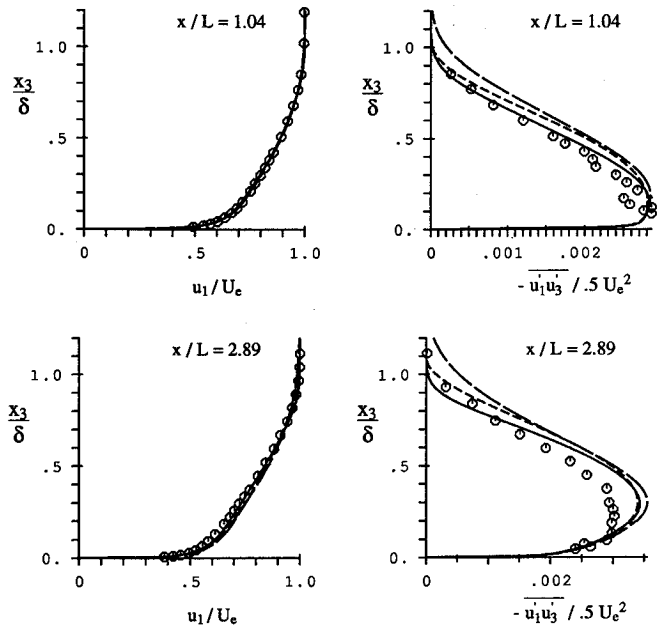

Fig. 3 SAJO73: mean velocity and Reynolds stress profiles; models: CF, ————; BL, — — —; MI, ----------.

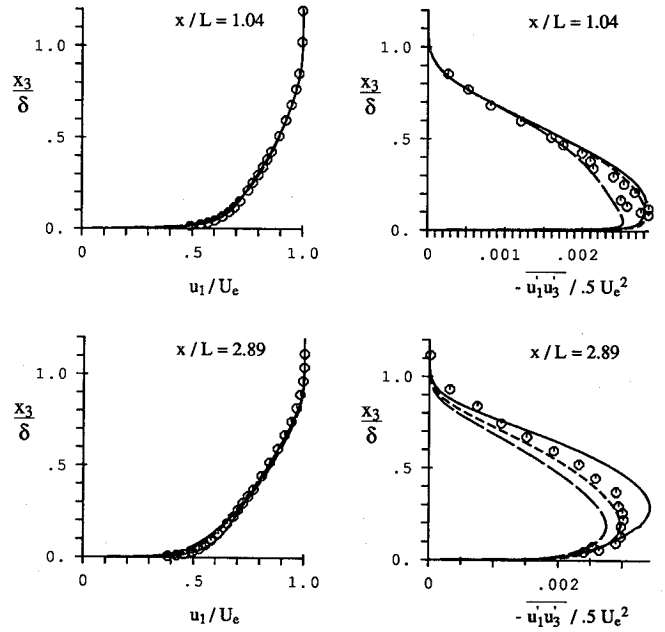

Fig. 4 SAJO73: mean velocity and Reynolds stress profiles; models: CF, ————; JK, — — —; JK2, ----------.

model used. The calculated Reynolds shear stresses at the first station, where the pressure gradient is small, are in better agreement with the experimental data than at the second. As the adverse pressure gradient becomes more pronounced further downstream, the Reynolds shear stresses predicted using the algebraic models are clearly too large, which in turn causes too high mean velocities in the inner part of the boundary layer. As a consequence, the predicted wall friction coefficient becomes too large and the displacement and momentum thicknesses too small (these parameters are not presented here). Similar results were obtained in all of the two-dimensional experiments with adverse pressure gradients considered in this study: SCKL50, CLAU54, SAJO73, and GATH92. When separation occurs, the location predicted is usually downstream of that observed. The differences in the predictions from the algebraic models tested are probably of little consequence in engineering work, but the excessive Reynolds shear stress obtained from the BL-model in the outermost part of the boundary layer should be noted. This effect has been observed also in the other test cases studied, and it is the reason why the BL-model is considered less satisfactory than other models tested herein.

The models JK and JK2 produce a somewhat reduced level of Reynolds shear stress, in better agreement with the experimental values. This leads to a significant improvement in the predictions of boundary layers subject to adverse pressure gradients. In the results presented in Fig. 4, JK2 is seen to be equivalent to CF at the first station but clearly superior at the second station, where the pressure gradient is more pronounced. The stress level computed using JK is too low at both stations, which is consistent with the results for the other two-dimensional test cases considered. This is clearly due to the eddy-viscosity distribution used in JK, which is better suited for boundary layers approaching separation. For such conditions, JK shows improved results, as shown in Johnson and King.[1]

In regions with moderately favorable or negligible pressure gradients (e.g., WITI44 and SCKL50), the algebraic models perform very well. For such flows JK2 is nearly equivalent to the simpler models, whereas JK is often inferior.

Selected results for the case BEEL72 are presented in Figs. 5–10. The definitions used for the integral boundary-layer thicknesses are

$$\delta_{11} = \int_0^\infty \left(1 - \frac{u_1}{U_e}\right) dx_3 \qquad \delta_{21} = \int_0^\infty \frac{u_1}{U_e}\left(1 - \frac{u_1}{U_e}\right) dx_3$$

$$\delta_{12} = -\int_0^\infty \frac{u_2}{U_e} dx_3 \qquad \delta_{22} = -\int_0^\infty \left(\frac{u_2}{U_e}\right)^2 dx_3$$

The results for the algebraic models are presented in Figs. 5 and 8. The predictions for the upstream part of the flowfield, where the crossflow is small, are in excellent agreement with the experimental data. With increasing three-dimensionality of the mean flow, i.e., with β_w larger than, say, 15 deg, the results deteriorate rapidly. In particular, the integral boundary-layer thicknesses, as well as β_w, are now too small. This can be attributed to the prescribed isotropy of the eddy viscosity, which gives too small crossflow, but also to the too high values for the streamwise eddy-viscosity component, as seen in Fig. 8. The results for the first station presented, i.e., $x/L \approx 0.8$, where the crossflow is small, are satisfactory, except for the crossflow component of the Reynolds shear stress, which is about twice as large as the experimental values. The station further downstream, i.e., $x/L \approx 1$, exhibits too large values for both Reynolds stress components, which in turn produce an excessive streamwise mean-velocity component and a too small crossflow. The behavior of the streamwise component is consistent with the observations made for two-dimensional boundary layers with adverse pressure gradients. The underprediction of the crossflow is caused both by the excessive streamwise mean velocity component, which reduces the imbalance between the centrifugal force and the lateral pressure gradient, and by the excessive Reynolds shear stress in the crossflow direction (in comparison with experiments), which reduces the crossflow. The results for CF and MI are in this respect nearly equivalent, whereas the use of BL gives less satisfactory predictions.

Figures 6 and 9 show the solutions obtained using JK and JK2. The results for the CF-model are also plotted in these figures to serve as reference. The solutions for the upstream part of the flowfield are nearly equivalent to those obtained using the algebraic models (Fig. 5 and 8) and are in good agreement with the experimental data. But with larger crossflows, important improvements are observed. Larger integral thicknesses are predicted, in good agreement with the experimental data. The best results are here due to JK, but this

model performs less satisfactorily in predicting the magnitude and the direction of the wall shear force. In particular, too high values of β_w over most of the computed range are observed. The mean velocity and Reynolds stress profiles are presented in Fig. 9. Again, with increasing crossflow, the quality of the predictions deteriorates, but certain improvements relative to the algebraic models are observed. As isotropy of the eddy viscosity is prescribed, the Reynolds stresses in the crossflow direction are consistently too high, but this effect is weakened by the overall reduction of the eddy viscosity magnitude. The streamwise components of the Reynolds shear stresses are well predicted by JK2, whereas the values resulting from JK are too small. This is consistent with the observations made for the two-dimensional cases with adverse pressure gradient.

The anisotropic formulation JK3 is compared with JK2 and with the experimental data in Figs. 7 and 10. As the magnitude of the maximum resulting Reynolds shear stress is computed using the original JK transport equation, also used in JK2, the results for streamwise components of the mean velocity and the Reynolds shear stress are practically unchanged. For both $T = 1$ and .75 the crossflow Reynolds shear stress is substan-

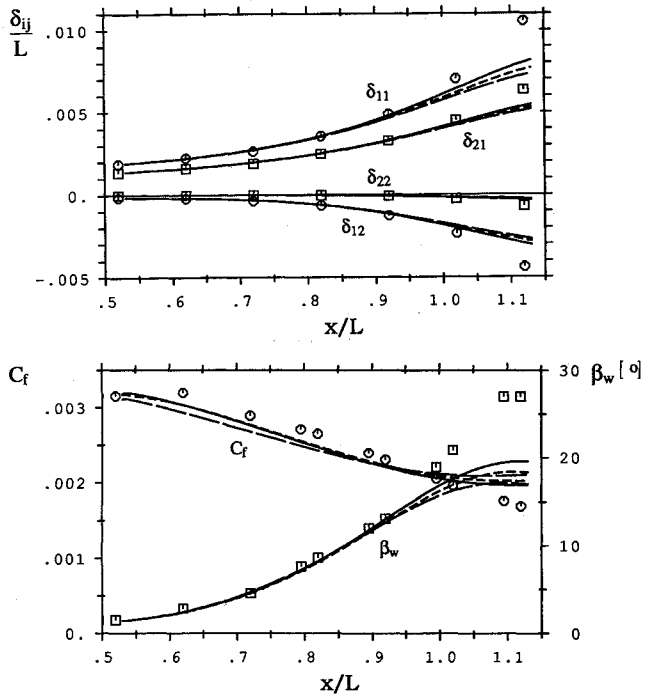

Fig. 5 BEEL72: integral boundary-layer thicknesses and wall friction coefficient; models: CF, ————; BL, — — —; MI, - - - - - - - - -.

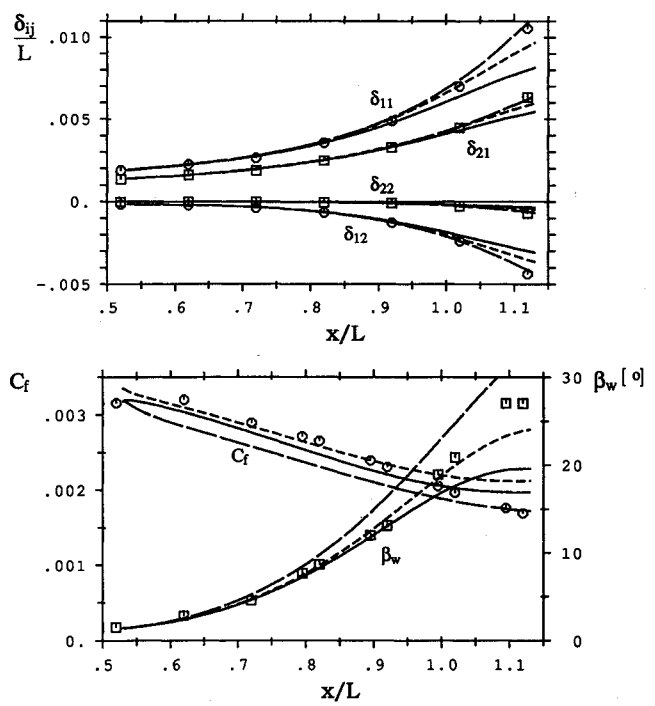

Fig. 6 BEEL72: integral boundary-layer thicknesses and wall friction coefficient; models: CF, ————; JK, — — —; JK2, - - - - - - - - -.

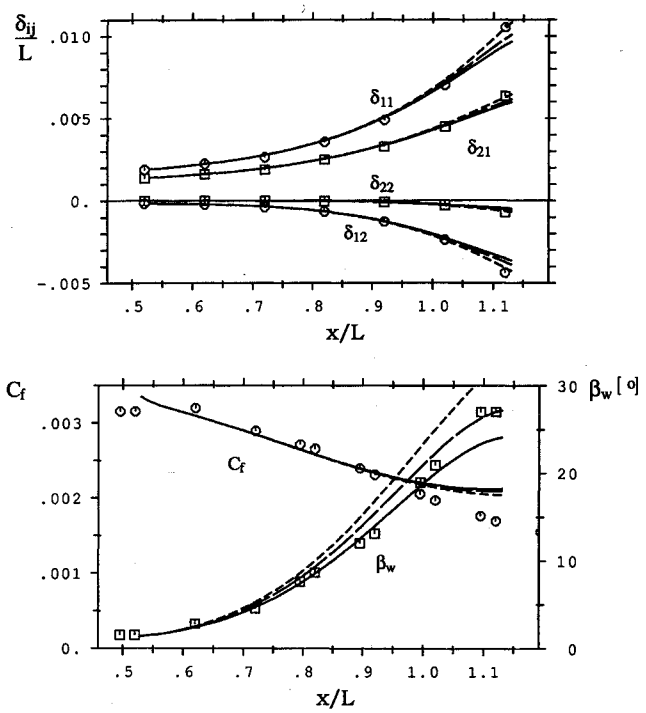

Fig. 7 BEEL72: integral boundary-layer thicknesses and wall friction coefficient; models: JK2, ————; JK3, $T = 1$, — — —; JK3, $T = 0.75$, - - - - - - - - -.

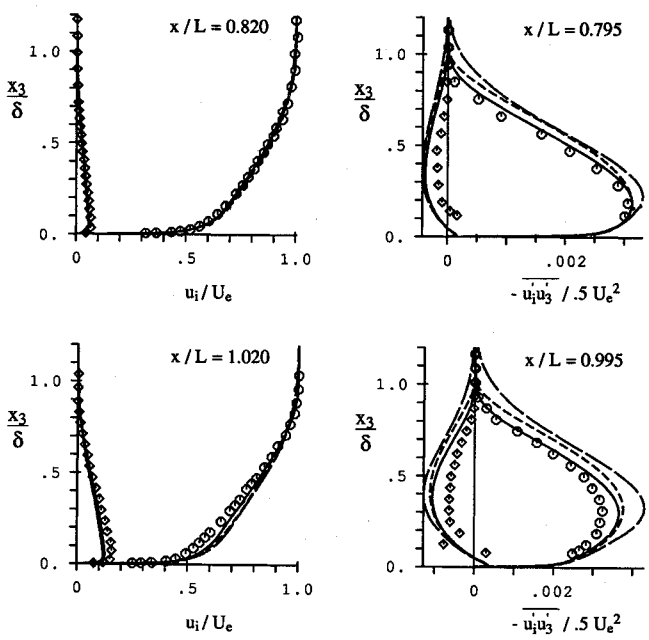

Fig. 8 BEEL72: mean velocity and Reynolds stress profiles; models: CF, ————; BL, — — —; MI, - - - - - - - - -.

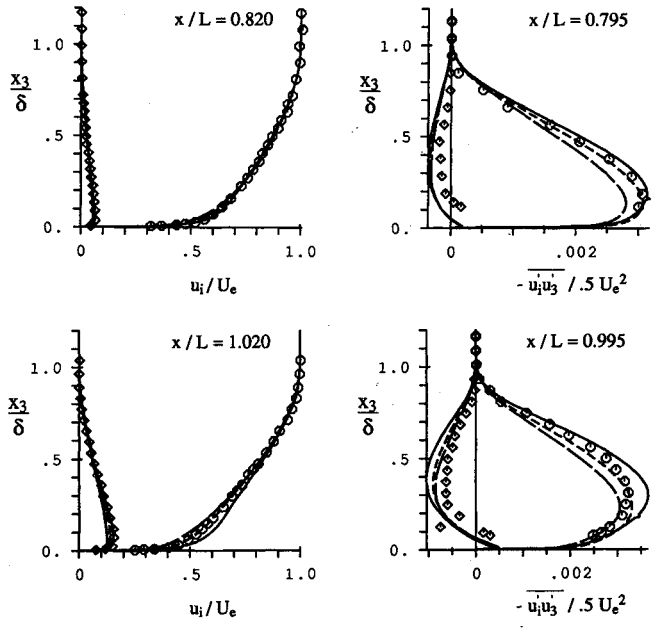

Fig. 9 BEEL72: mean velocity and Reynolds stress profiles; models: CF, ————; JK, — — —; JK2, - - - - - - - - -.

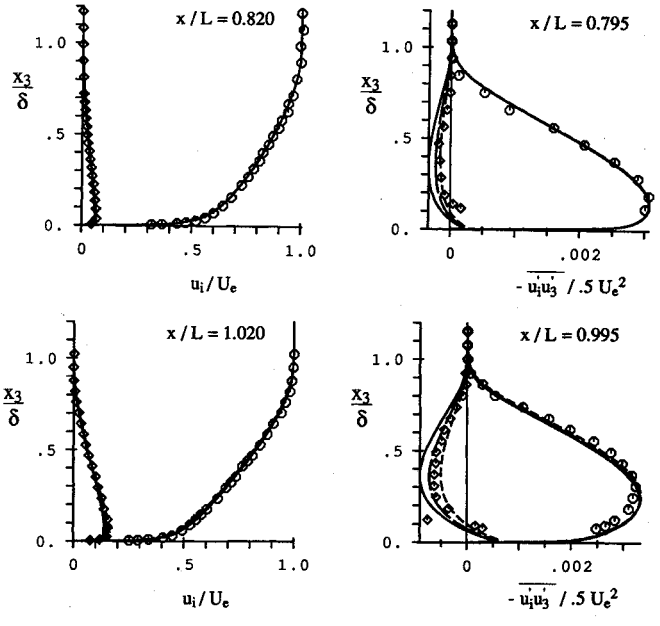

Fig. 10 BEEL72: mean velocity and Reynolds stress profiles; models: JK2, ————; JK3, $T = 1$, — — —; JK3, $T = 0.75$, - - - - - - - - -.

tially reduced and found to be in excellent agreement with the experimental data. The mean velocity profiles agree with the experimental values within the experimental accuracy. The integral boundary-layer thicknesses are best predicted using $T = .75$, whereas β_w compares better with the experimental data if $T = 1$ is used. As separation is approached, too high values of C_f are predicted, as with all of the models but JK. The resulting distributions of the anisotropy parameter A are presented in Fig. 11.

The comparison with the POBR82 data leads to the same conclusions, but for details. The conclusions for the remaining pressure-driven cases listed in Table 3 are less clear. In the two wing-body-junction flows, DEFE77 and KRFA79, it appears that the turbulence models have only a minor influence on the mean velocity field, which is dominated by pressure gradients. In fact, the mean velocity field is well predicted by all of the

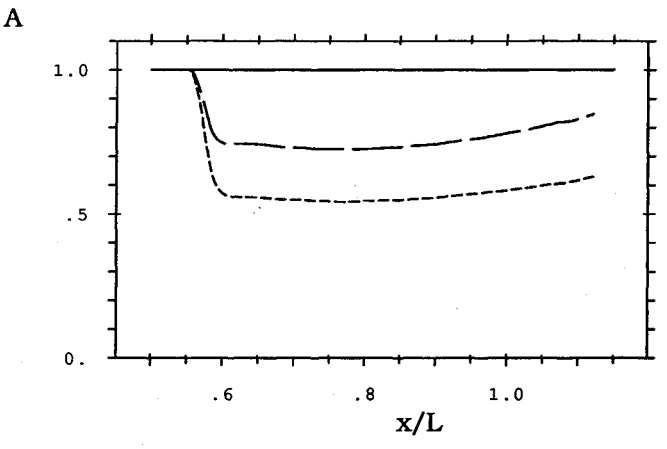

Fig. 11 BEEL72: variation of the anisotropy parameter A; models: JK2, ————; JK3, $T = 1$, — — —; JK3, $T = 0.75$, - - - - - - - - -.

models tested, although in some regions the resulting Reynolds shear stresses are in poor agreement with the experimental data. For this reason it appears to be preferable to use algebraic models in such situations. In these cases, as well as in MUKR79 and TRRY90, the complex external velocity distribution could be responsible for additional errors in the computational results, due to the incomplete knowledge of the external boundary conditions.

The main features of the shear-driven flows BIME70 and LOHM73 are well captured by all of the algebraic models investigated. The use of JK and JK2 leads here only to minor changes.

As a part of our research work, the models for the eddy-viscosity anisotropy presented in Table 2 have also been tested, in combination with the algebraic models, JK and JK2. The Ryhming-Fanneløp formulation, which does not involve additional model parameters, is applicable in its present form only to the near-wall region of the boundary layer. For this reason the predicted effect of anisotropy is in most cases too small. The remaining formulations listed in Table 2 can lead to improved results in good agreement with the experimental data, provided suitable values for the empirical anisotropy parameters can be determined. These results are presented and further discussed in Bettelini.[15] For Fanneløp-Humphreys' and Rotta's models, a constant value will often be sufficient, but the use of a constant B in Moreau's model seems to be too crude an approximation. The best results have been obtained when the models are combined with the JK2 formulation. When used in combination with the algebraic models, the results are improved in comparison with the isotropic versions of the same models, but the resulting Reynolds shear stresses are often too high. In the new formulation JK3, the anisotropy parameter A is computed at every location and depends on the upstream flowfield. The parameter T must be specified in advance, but this is expected to be less critical than the determination of the A distribution. More research is required to determine the range of applicability of this model and to see if the parameter T has a universal and not a flow-specific character.

VI. Conclusions

The present study confirms that the more widely used and mathematically simpler turbulence models give acceptable predictions for a variety of pressure-driven boundary layers, in the absence of flow separation.

The performance is less satisfactory for flows with adverse pressure gradients (in both two and three dimensions) and in cases involving large crossflows. In the three-dimensional case the deterioration in performance can be attributed both to neglect of anisotropy, present in experiments, and to overpre-

diction of the eddy viscosity. The use of the CF-model is a good choice among the algebraic models tested. The BL-model gives never better, but sometimes less satisfactory results, and its use should be restricted to the cases for which this formulation is required, e.g., for Navier-Stokes solutions in the presence of small separated regions.

Models of the JK class are found to improve the results for both adverse pressure gradients and for cases with strong three-dimensional effects. Compared with the JK model, the eddy-viscosity distribution used in the JK2 model is found to be in better agreement with most of the experimental data considered herein. It should be recalled that the present experimental basis includes largely flows well upstream of separation. Both models JK and JK2 are believed to be well suited for engineering applications. The choice will depend on the type of flow, i.e., far away from or approaching separation.

Among the simpler models for eddy-viscosity anisotropy tested herein, the formulations proposed by Fanneløp-Humphreys and Rotta are found to give the best results. In both cases an additional anisotropy parameter has to be specified. This presents a major problem in many practical situations. To avoid the necessity of specifying the anisotropy factors, a new extension of the Johnson-King model is proposed herein. In this new formulation the eddy-viscosity anisotropy is computed at each step and depends on the upstream flowfield. The initial results are promising as shown, but more work is required to assess the applicability of this model.

For the two shear-driven test cases considered herein, the simplest algebraic models work satisfactorily, and no benefit results when applying models of the Johnson-King class. Additional studies of shear-driven boundary-layer flows would be of interest.

References

[1]Johnson, D. A., and King, L. S., "A New Turbulence Closure Model for Attached and Separated Turbulent Boundary Layers," *AIAA Journal,* Vol. 23, No. 11, 1985, pp. 1684–1692.

[2]van den Berg, B., Humphreys, D. A., Krause, E., and Lindhout, J. P. F., "Three-Dimensional Turbulent Boundary Layers—Calculations and Experiments," *Notes on Numerical Fluid Mechanics,* Vol. 19, Vieweg Verlag, Braunschweig, Germany, 1987.

[3]Cebeci, T., and Smith, A. M. O., *Analysis of Turbulent Boundary Layers,* Academic Press, New York, 1974.

[4]Fanneløp, T. K., and Humphreys, D. A., "A Simple Finite-Difference Method for Solving the Three-Dimensional Turbulent Boundary Layer Equations," AIAA Paper 74-13, Jan. 1974.

[5]Baldwin, B., and Lomax, H., "Thin-Layer Approximation and Algebraic Model for Separated Turbulent Flows," AIAA Paper 78-257, Jan. 1978.

[6]Michel, R., Quémard, C., and Durant, R., "Hypotheses on the Mixing Length and Application to the Calculation of the Turbulent Boundary Layers," edited by S. J. Kline, M. Morkovin, G. Sovron, and D. J. Cockrell, *Proceedings of the 1968 AFOSR-IPF-Stanford Conference,* Stanford Univ., Stanford, CA, 1968.

[7]Abid, R., "Extension of the Johnson-King Turbulence Model to 3-D flows," AIAA Paper 88-0223, Jan. 1988.

[8]Ryhming, I. L., and Fanneløp, T. K., "A 3D Law of the Wall Including Skewness and Roughness Effects," *Proceedings of the IUTAM Symposium on Three-Dimensional Boundary Layers,* Springer-Verlag, Berlin, 1982, pp. 325–342.

[9]Rotta, J. C., "A Family of Turbulence Models for Three-Dimensional Boundary Layers," *Selected Papers from the First International Symposium on Turbulent Shear Flows,* Springer-Verlag, Berlin, 1977.

[10]Rotta, J.C., "On the Effect of the Pressure Strain Correlations on Three-dimensional Turbulent Boundary Layers," *Proceedings of the Second International Symposium on Turbulent Shear Flows,* Springer-Verlag, London, 1979, pp. 266–278.

[11]Moreau, V., "A Study of Anisotropic Effects in Three-dimensional, Incompressible Turbulent Boundary Layers Driven by Pressure Gradients," Ph.D. Thesis, Swiss Federal Institute of Technology, Lausanne, Switzerland, 1989.

[12]Johnston, J. P., "Experimental Studies in 3D Turbulent Boundary Layers," Stanford Univ., Rept. MD-34, Stanford, CA, July, 1976.

[13]Lighthill, M. J., "On Displacement Thickness," *Journal of Fluid Mechanics,* Vol. 4, Pt. 4, Aug. 1958, pp. 383–392.

[14]Fanneløp, T. K., "Displacement Thickness for Boundary Layers with Mass Transfer," *AIAA Journal,* Vol. 4, No. 6, 1966, pp. 1142–1144.

[15]Bettelini, M. S. G., "Numerical Study of Some Engineering Turbulence Models for Three-Dimensional Boundary Layers," Ph.D. Thesis, Swiss Federal Institute of Technology, Zürich, Switzerland, 1990.

[16]Wieghardt, K., and Tillmann, W., "Zur turbulenten Reibungsschicht bei Druckgradient," *Proceedings of the 1968 AFOSR-IPF-Stanford Conference,* U&M 6617, Vol. II, 1944, pp. 98–123.

[17]Schubauer, G., and Klebanoff, P., "Investigation of Separation of the Turbulent Boundary Layer," NACA TR 1030, 1951.

[18]Clauser, F., "Turbulent Boundary Layer in Adverse Pressure Gradients," *Journal of Aeronautical Sciences,* Vol. 21, Feb. 1954, pp. 91–108.

[19]Samuel, A. E., and Joubert, P. N., "A Boundary Layer Developing in an Increasing Adverse Pressure Gradient," *Journal of Fluid Mechanics,* Vol. 66, Pt. 3, Nov. 1974, pp. 481–505.

[20]Gasser, D., "Turbulente Grenzschicht mit starkem Druckgradient," Ph.D. Thesis, Swiss Federal Institute of Technology, Zürich, Switzerland, 1992.

[21]van den Berg, B., Elsenaar, A., Lindhout, J. P. F., and Wesseling, P., "Measurements in an Incompressible Three-Dimensional Turbulent Boundary Layer, Under Infinite Swept-Wing Conditions, and Comparison with Theory," *Journal of Fluid Mechanics,* Vol. 70, Pt. 1, July 1975, pp. 127–148.

[22]Bradshaw, P., and Pontikos, N. S., "Measurements in the Turbulent Boundary Layer on an "Infinite" Swept Wing," *Journal of Fluid Mechanics,* Vol. 159, Oct. 1985, pp. 105–130.

[23]Dechow, R., and Felsch, K. O., "Measurements of the Mean Velocity and of the Reynolds Stress Tensor in a Three-Dimensional Turbulent Boundary Layer Induced by a Cylinder Standing on a Flat Wall," *Proceedings of the First International Symposium on Turbulent Shear Flows,* Springer-Verlag, Berlin, 1977.

[24]Felsch, K. O., Paulsen, L., and Schulenberg, T., "Experimentelle Untersuchung der three-dimensional turbulenten Grenzschicht vor einem senkrecht auf einer ebenen Wand stehenden Zylinder," Fortschr.-Ber. VDI-Z., Reihe 7, No. 79, VDI Verlag, Düsseldorf, Germany, 1983.

[25]Krogstad, P. A., "Investigation of a Three-Dimensional Turbulent Boundary-Layer Driven by a Simple Two-Dimensional Potential Flow," Ph.D. Thesis, Norwegian Institute of Technology, Trondheim, Norway, 1979.

[26]Müller, U. R., "Measurement of the Reynolds Stress and the Mean Flow Field in a Three-Dimensional Pressure-Driven Boundary Layer," *Journal of Fluid Mechanics,* Vol. 119, June 1982, pp. 121–153.

[27]Truong, T. V., and Brunet, M., "Test case T: Boundary Layer in a 'S'-Shaped Channel," edited by O. Piranneau, W. Radi, I. L. Rhyming, A. N. Savill, and T. V. Truang, *Proceedings of the ERCOFTAC Workshop on Numerical Simulation of Unsteady Flows, Transition to Turbulence and Combustion,* (Cambridge University Press), EPF, Lausanne, Switzerland, 1992, pp. 78–115.

[28]Bissonnette, L. R., and Mellor, G. L., "Experiments on the Behavior of an Axisymmetric Turbulent Boundary Layer with a Sudden Circumferential Strain," *Journal of Fluid Mechanics,* Vol. 63, Pt. 2, April, 1974, pp. 369–413.

[29]Lohmann, R. P., "The Response of a Developed Turbulent Boundary Layer to Local Transverse Surface Motion," *Transactions of the ASME: Journal of Fluids Engineering,* Vol. 98, Sept. 1976, pp. 354–363.

[30]Fanneløp, T. K., "A Method for Solving the Three-Dimensional Laminar Boundary-Layer Equations with Application to a Lifting Reentry Body," *AIAA Journal,* Vol. 6, No. 6, 1968, pp. 1075–1084.